Supporting Information

on

Ni Nanoparticles Coated with Nitrogen-Doped Carbon for Optical Limiting Applications

Rajeev Kumar[a], Ajay Kumar[b], Nancy Verma[b], Vijay Khopkar[a], Reji Philip[b] and Balaram Sahoo[a,*]

[a]*Materials Research Centre, Indian Institute of Science, Bangalore-560012, India*

[b]*Raman Research Institute, Bangalore-560080, India*

[*]*Corresponding author's email:* bsahoo@iisc.ac.in

Z-scan measurements

5 mg sample was sonicated in 1 ml of ethylene glycol. 20 μl of the dispersed sample was pipetted out and redispersed in 0.98 ml of ethylene glycol. For the Z-scan experiment, the fluid was again sonicated and the stable dispersion was taken in a quartz cuvette (1 mm path length). The cuvette was placed on a linear translational stage with automated stepper motor controls. 532 nm pulsed laser of 40 μJ (5 ns pulse width) were irradiated on the sample. Experiments were also performed at input energies of 10, 20 and 60 μJ. The linear transmittance was 80 ± 5% for all the Z-scans. The pulse repetition frequency was kept low (1 Hz) to avoid collective thermal effects in the fluid. The laser beam was focussed using a plano-convex lens (6.29 cm focal length). The focal point at z = 0 corresponds to maximum energy density (fluence) and reduces progressively towards either side of it, considering laser beam propagation direction along z-axis. The laser beam radius $w(z)$ at each beam position (z) is obtained by equation (1) :

$$w(z) = w_0\sqrt{1+\left(\frac{z}{z_0}\right)^2} \qquad (1)$$

where, w_0 is the beam radius at focal point (z = 0), w_0 = 14 μm as obtained from knife edge measurements and $z_0 = \frac{\pi w_0^2}{\lambda}$ is the Rayleigh range. The different input beam peak intensity is obtained from the expression: $I_{\text{int}} = \frac{4\sqrt{\ln 2}}{\pi^{3/2}}\frac{E_{in}}{\left(w(z)\right)^2 \delta t}$, where E_{in} is input laser pulse energy (40 μJ) and δt is the width of the laser pulse (5 ns). The transmittance versus (z) yields the open aperture Z-scan curves, from which various relevant non-linear optical coefficients are extracted.

Table S1. The crystallite size and the relative percentage (composition) of amorphous type carbon phase (graphite-1, G1) and graphite phase (graphite-2, G2) in the synthesized samples. The estimated error bars for each parameter is also given.

Sample	Peak position 2θ(°)		Composition (%)		Crystallite size (nm)	
	G1 (± 0.05)	G2 (± 0.05)	G1 (± 2)	G2 (± 2)	G1 (± 0.5)	G2 (± 0.5)
Ni-250-1	23.17	26.31	56.2	43.8	1.01	3.03
Ni-250-3	23.40	26.36	55.4	44.6	1.06	3.04
Ni-250-10	23.99	26.39	41.7	58.3	1.07	4.01
Ni-250-20	23.39	26.23	36.9	63.1	1.05	3.85

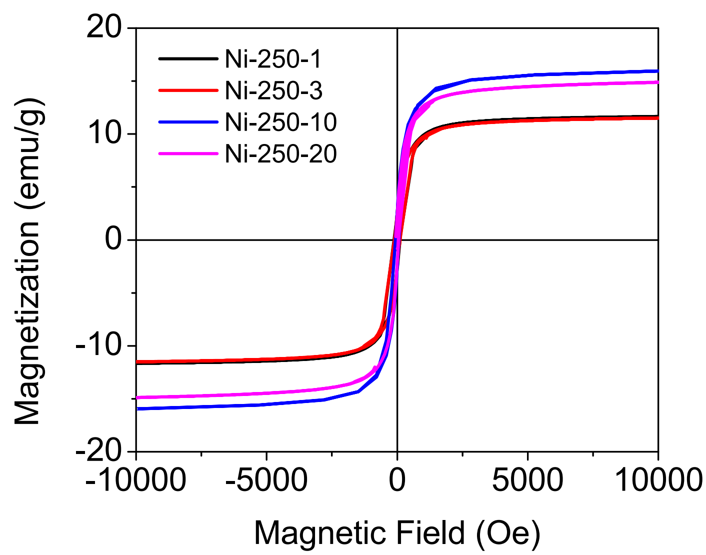

Figure S1. VSM plots of the Ni@C samples.

Table S2. M versus H parameters.

Sample	Saturation magnetization, M_s (emu/g)	Coercivity, H_c (Oe)
Ni-250-1	11.7	180
Ni-250-3	11.5	111
Ni-250-10	15.9	72
Ni-250-20	14.9	59

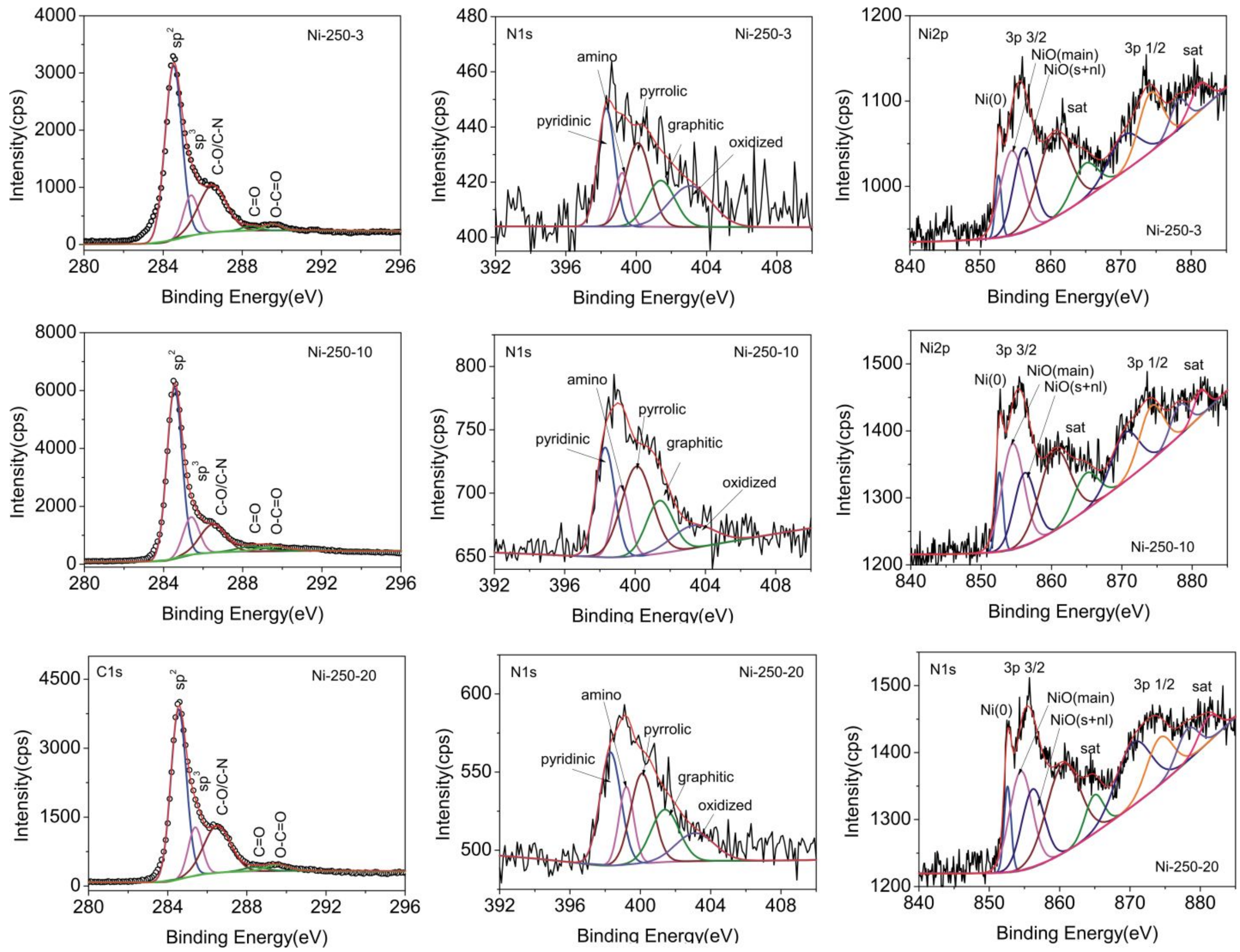

Figure S2. C 1s spectra (left panel), N 1s (middle panel) and Ni 2p spectra (right panel) of the Ni-250-3, Ni-250-10 and Ni-250-20 samples.

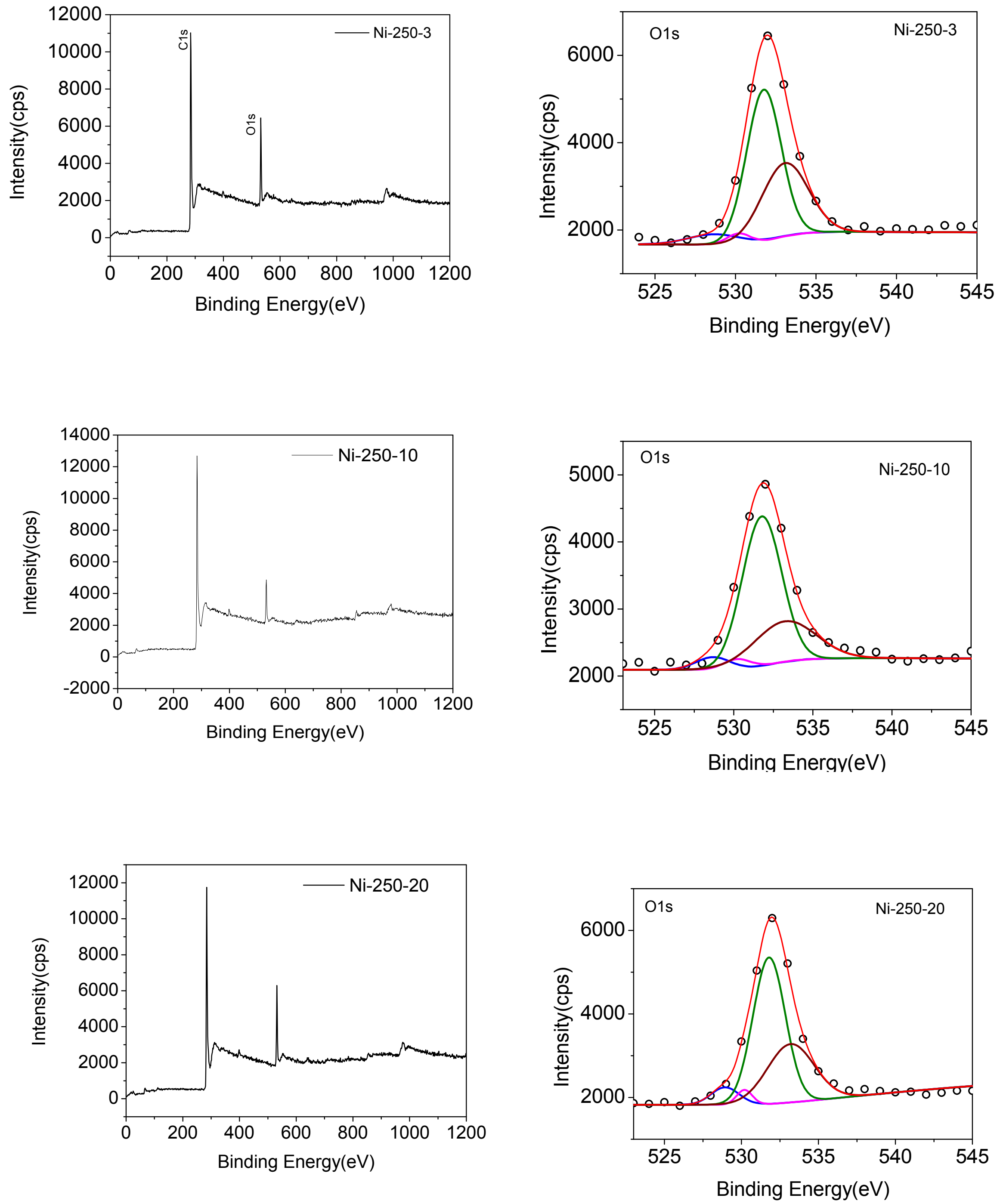

Figure S3. (left panel) Wide XPS spectra depicting the entire range of binding energies for all the studied samples. (right panel) O1s spectra for all the studied samples.

Table S3. Assignment of the binding energies to the various functionalities corresponding to C1s, N1s and Ni2p XPS spectra.

XPS sub spectra	Assignment	Binding energy (eV)	Relative Percentage		
			Ni-250-3	Ni-250-10	Ni-250-20
C1s	sp^2	284.6	58.8	61.8	54.9
	sp^3	285.4	11.5	14.2	13.7
	C-O/C-N	286.5	26.0	17.3	26.5
	C=O	288.4	1.6	3.4	1.9
	O-C=O	289.5	2.1	3.3	3.0
N1s	Pyridinic	398.3	25.4	24.9	29.1
	Amino	399.2	9.6	13.9	14.1
	Pyrrolic	400.1	26.5	32.8	25.4
	Graphitic	401.4	16.6	16.8	19.1
	Oxidized N	403.0	21.9	11.6	13.3
Ni2p	Metal (0)	852.6	3.4	4.9	4.7
	Ni2p 3/2 (main)	854.5	17.3	20.8	17.4
	Ni2p 3/2 (surface+ non-local)	856.2	15.6	13.7	13.6
	Ni2p 3/2 satellite	860.5	24.0	21.5	23.1
		864.9	7.8	7.9	5.4
	Ni2p 1/2 (main)	870.5	10.1	11.9	16.9
	Ni2p 1/2 (surface+ non-local)	874.2	12.7	11.4	9.6
	Ni2p 1/2 satellite	878.2	4.5	4.8	5.3
		881.2	4.6	3.1	4.0
O1s	NiO	528.7	5.7	4.7	5.9
	Ni-O-C	530.2	2.6	3.0	2.8
	C=O	531.8	55.6	64.7	57.9
	C-OH/C-O-C	533.2	36.1	27.6	33.3

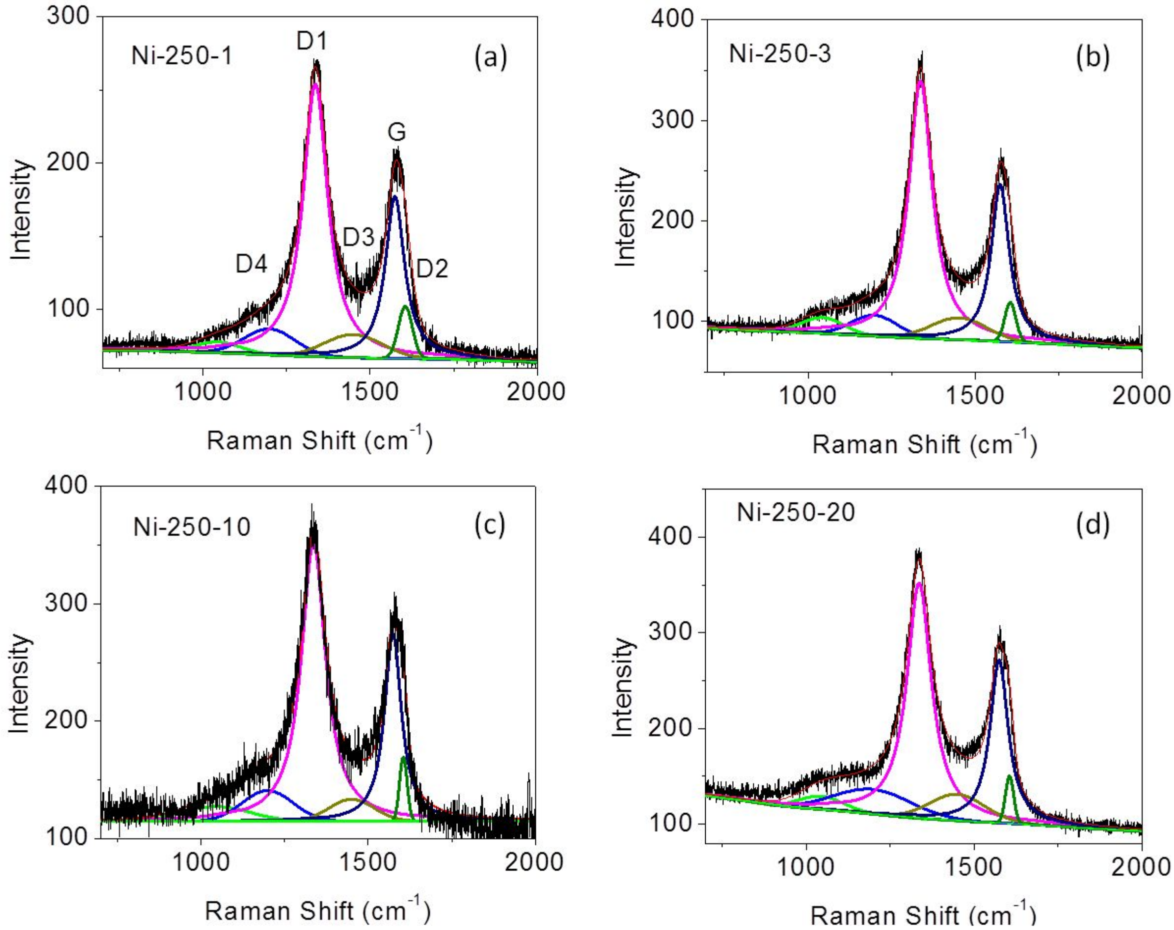

Figure S4. (a) Raman spectra of Ni-250-1, Ni-250-3, Ni-250-10 and Ni-250-20 samples. (b) Zoomed-in view of the Raman spectra for all the samples showing the region where the NiO peak appears. (c-f) The individual picture of the deconvoluted D and G Raman peaks, for all the samples.

Table S4. Assignment of the Raman peaks.

Peak Position (cm^{-1})	Peak designation	Peak origin
1570-1590	G	Crystalline graphitic carbon
1335-1345	D1	C=C structural defects (in-plane breathing vibrations of sp^2-bonded carbon within structural defects)
1600-1610	D2	Edge defects in graphitic crystallites
1460-1480	D3	Defects in amorphous carbon
1190-1200	D4	sp^2-sp^3 bonds or C−C and C=C stretching vibrations of polyenes or conjugated system

Table S5. Relative intensity ratios derived from the fits of the Raman spectra.

Sample	I_G/I_D	I_G/I_{D2}	I_G/I_{D3}
Ni-250-1	0.151	1.55	0.89
Ni-250-3	0.154	1.90	0.82
Ni-250-10	0.153	1.90	1.05
Ni-250-20	0.155	1.91	0.86

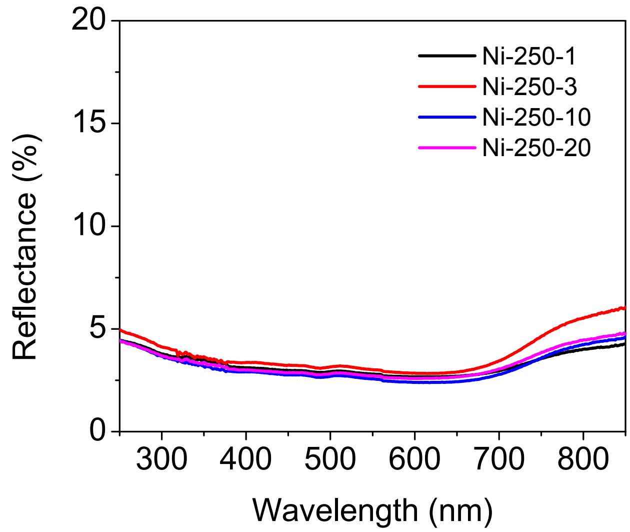

Figure S5. (a) UV-Vis DRS (Reflectance versus wavelength) plots for of Ni-250-1, Ni-250-3, Ni-250-10 and Ni-250-20 samples.

Urbach energy calculations : E_u = 1/slope (Figure S6)

For, Ni-250-1: $E_u = 1/(1.5675) = 638$ meV

For, Ni-250-3: $E_u = 1/(2.5181) = 397$ meV

For, Ni-250-10: $E_u = 1/(5.6832) = 176$ meV

For, Ni-250-20: $E_u = 1/(2.1526) = 464$ meV

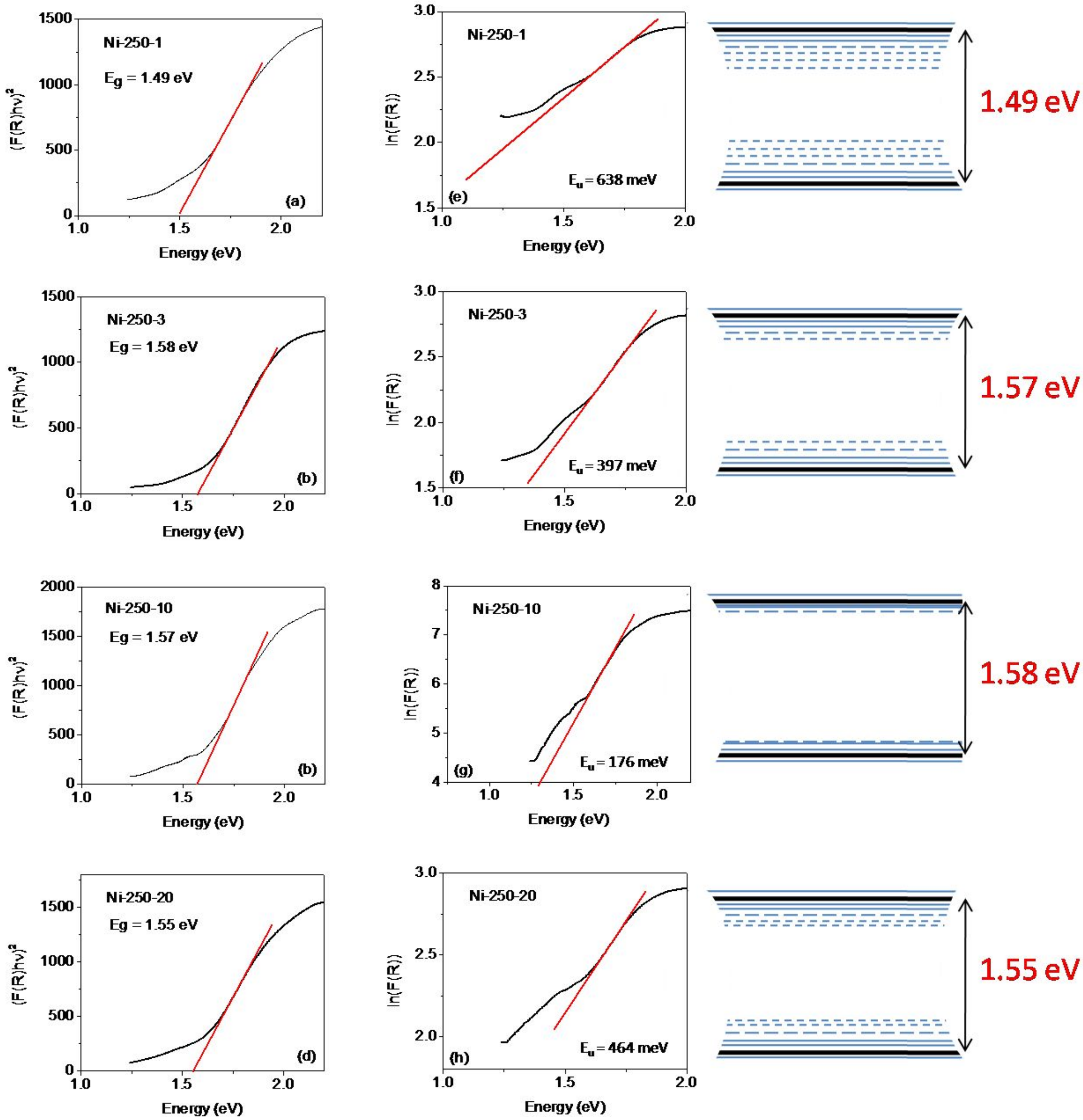

Figure S6. (a-d) Kubelka-Munk function (F(R)) versus energy (hν) plots for of Ni-250-1, Ni-250-3, Ni-250-10 and Ni-250-20 samples. (e-h) The ln(F(R)) versus energy (hν) plots used for the determination of the Urbach energy (E_u). The right panel shows the cartoon representing the energy band structure shown considering the obtained Urbach energy.

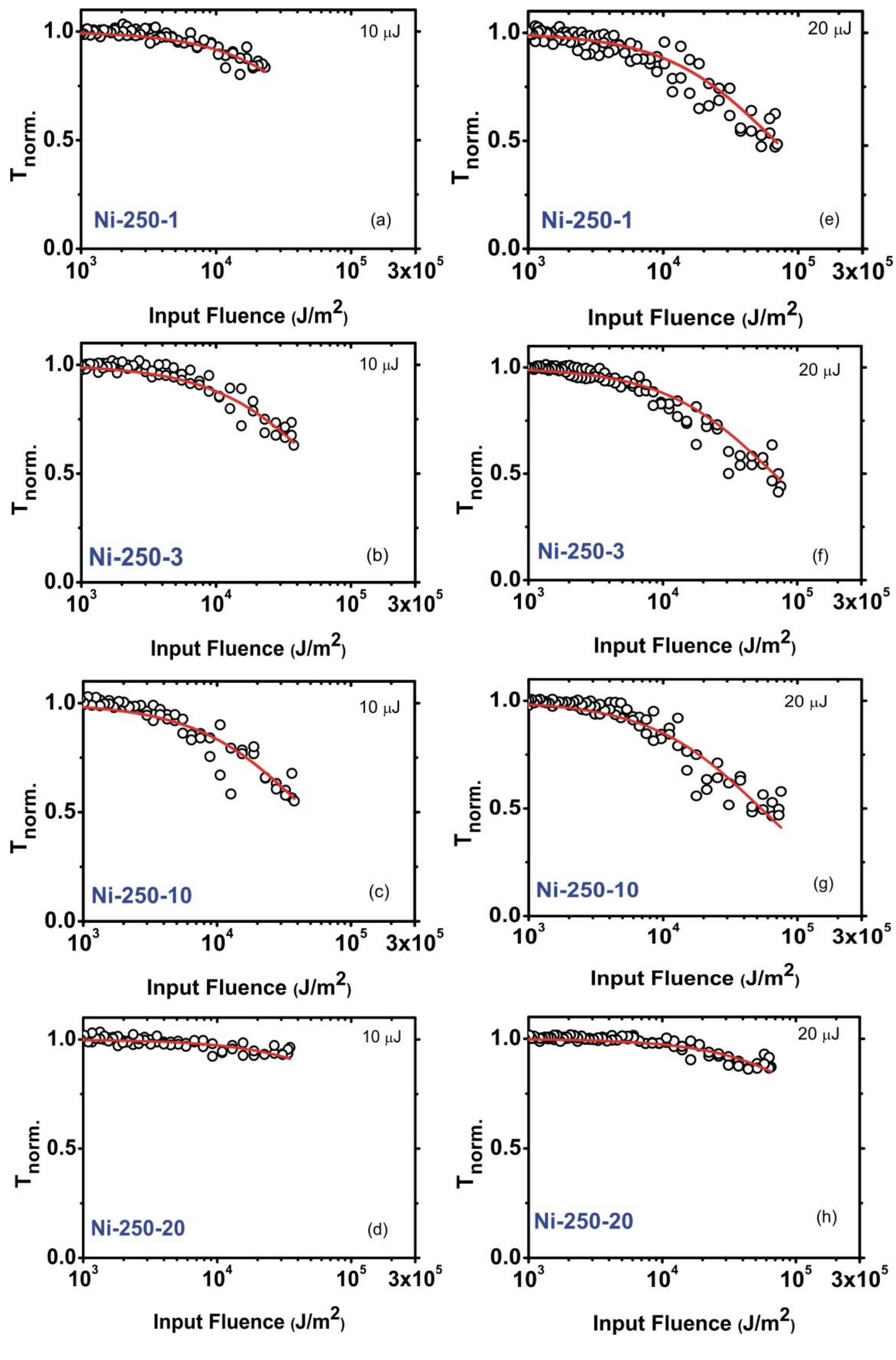

Figure S7. Normalized transmittance versus Fluence for the synthesized samples: (left panel, a-d) at 10 μJ and (right panel, e-h) 20 μJ input energies, respectively.

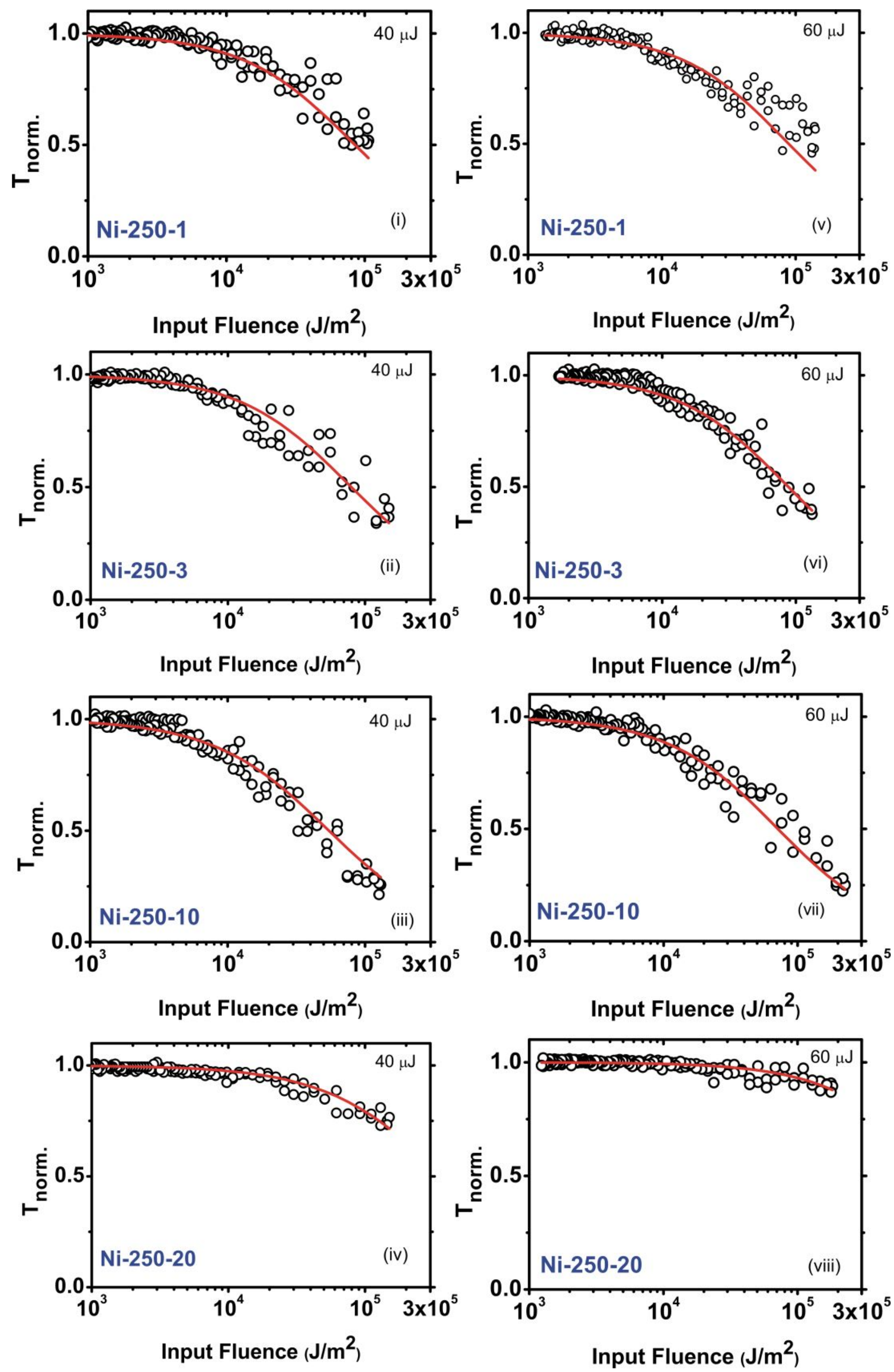

Figure S8. Normalized transmittance versus Fluence for the synthesized samples: (left panel, i-iv) at 40 μJ and (right panel, v-viii) 60 μJ input energies, respectively.

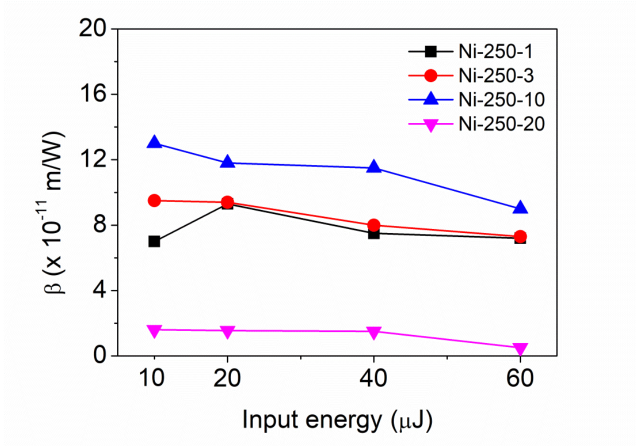

Figure S9. Variation of *β* versus input energy for the synthesized samples.

Table S6. Comparison of OL performance of the synthesized Ni-250-10 samples with standard materials.

Sample	Input Energy (μJ)	Pulse	Wavelength (nm)	LT%	*β* (m/W)	OL threshold (J/cm^2)	Ref.
MWCNT in H_2O	-	7 ns	532	50	-	1	1
rGO	-	5 ns	532	-	2.8×10^{-10}	8.3	2
SWCNT in H_2O	-	5 ns	532	24	-	0.15	3
GO	71.56	5 ns	532	-	10^{-10}	1.80	4
C_{60}	-	8 ns	532	65	-	0.2	5
C_{60}	-	6 ns	532			0.36	6
GO-ZnS (4:5)	-	340 fs	1030	78	5.55×10^{-6}	0.97	7
f-MWCNT	185	5 ns	532	70	-	0.37	8
Ni-250-10	40	5 ns	532	80	11.5×10^{-11}	5.56	This work

References

(1) Sun, X.; Yu, R. Q.; Xu, G. Q.; Hor, T. S. A.; Ji, W. Broadband Optical Limiting with Multiwalled Carbon Nanotubes. *Appl. Phys. Lett.* **1998**, *73*, 3632–3634. https://doi.org/10.1063/1.122845.

(2) Sakho, E. hadji M.; Oluwafemi, O. S.; Sreekanth, P.; Philip, R.; Thomas, S.; Kalarikkal, N. Improved Nonlinear Optical and Optical Limiting Properties in Non-Covalent Functionalized Reduced Graphene Oxide/Silver Nanoparticle (NF-RGO/Ag-NPs) Hybrid. *Opt. Mater.* **2016**, *58*, 476–483. https://doi.org/10.1016/j.optmat.2016.06.030.

(3) Vivien, L.; Lancon, P.; Hache, F.; Riehl, D.; Anglaret, E. Pulse Duration and Wavelength Effects on Optical Limiting Behaviour in Carbon Nanotube Suspensions. *Conf. Lasers Electro-Optics Eur. - Tech. Dig.* **2000**, *26*, 187. https://doi.org/10.1109/cleoe.2000.910017.

(4) Cai, S.; Zheng, C.; Xiao, X.; Li, W.; Chen, W. Graphene-Based Hierarchical Sandwich-Type Hybrid Nanostructures for Optical Limiters. *Opt. Mater.* **2019**, *98*, 109453. https://doi.org/10.1016/j.optmat.2019.109453.

(5) Qu, S.; Chen, Y.; Wang, Y.; Song, Y.; Liu, S.; Zhao, X.; Wang, D. Enhanced Optical Limiting Properties in a Novel Metallophthalocyanine Complex $(C_{12}H_{25}O)_8PcPb$. *Mater. Lett.* **2001**, *51*, 534–538. https://doi.org/10.1016/S0167-577X(01)00351-2.

(6) Justus, B. L.; Kafafi, Z. H.; Huston, A. L. Excited-State Absorption-Enhanced Thermal Optical Limiting in C_{60}. *Opt. Lett.* **1993**, *18*, 1603–1605. https://doi.org/10.1364/OL.18.001603.

(7) Li, P. ling; Wang, Y. hua; Shang, M.; Wu, L. fu; Yu, X. X. Enhanced Optical Limiting Properties of Graphene Oxide-ZnS Nanoparticles Composites. *Carbon* **2020**, *159*, 1–8. https://doi.org/10.1016/j.carbon.2019.12.013.

(8) Anand, B.; Addo Ntim, S.; Sai Muthukumar, V.; Siva Sankara Sai, S.; Philip, R.; Mitra, S.

Improved Optical Limiting in Dispersible Carbon Nanotubes and Their Metal Oxide Hybrids. *Carbon* **2011**, *49* (14), 4767–4773. https://doi.org/10.1016/j.carbon.2011.06.086.